

# Quantitative Electron Microscopy Using Digital Data Processing

Kazuo Ishizuka<sup>†</sup> and Eiji Okunishi<sup>††</sup>

<sup>†</sup>HREM Research Inc

<sup>††</sup>Electron Optics Division, JEOL Ltd.

---

Digital equipments for electron microscopy, such as a CCD camera, come into wide use, and performance of a personal computer becomes more powerful than that of a main computer a decade ago. Thus, quantitative electron microscopy becomes a reality, where digital data obtained by using an electron microscope is analyzed quantitatively. Quantitative electron microscopy makes it possible to deduce information from an observed data, which is hard to be detected before by using human eyes. This report will introduce quantitative electron microscopy by making use of the data taken with JEOL JEM-2100F using some of the plug-ins developed at HREM Research for DigitalMicrograph (Gatan).

## Introduction

Current hot topics of high-resolution electron microscopy are high-resolution STEM-HAADF imaging and spherical aberration correction of an objective lens using a multi-poles corrector. There are two types of corrector, one is for a probe forming objective lens in a STEM mode, and the other is for an imaging objective lens in a CETM mode. When a spherical aberration is corrected, we can expect in principle an improvement of resolution. However, it does not simply mean that getting an atomic resolution image becomes easier using a Cs-corrected microscope than using a conventional microscope. Especially in a CETM mode a sample for high-resolution microscopy is well approximated as a phase object. Thus, when a spherical aberration is corrected in CETM, at a just defocus our sample only gives a weak scattering contrast (amplitude contrast). Furthermore, to realize an improvement of resolution we will be faced with unprecedented demands for stability of microscope and skills of operating a microscope and preparing a good sample.

On the other hand, digital equipments for

electron microscopy, such as a CCD camera, come into wide use, and performance of a personal computer becomes more powerful than that of a main computer a decade ago. Thus, quantitative electron microscopy becomes a reality, where digital data obtained by using an electron microscope is analyzed quantitatively. Quantitative electron microscopy may enhance periodic structure by reducing a periodic noise from an image; improve resolution of a STEM-HAADF image or an EELS spectrum using deconvolution technique; and measure lattice distortion from a single lattice image. Moreover, procedures to reconstruct a wave front and correct spherical aberration from a series of CETM images have been proposed [1-3], and corresponding software are now commercially available.

This report will introduce quantitative electron microscopy using plug-ins developed at HREM Research for DigitalMicrograph (Gatan [4]). Although we cannot introduce all of our plug-ins due to space limitations, we hope that we can demonstrate effectiveness of quantitative electron microscopy, and encourage the reader to apply quantitative microscopy on their data at hand.

## Resolution Improvement of STEM-HAADF Image

A STEM-HAADF image can be approxi-

mately expressed by using a convolution integral between an instrument function, a probe function here, and an object function [5]. Deconvolution is a procedure to estimate the object function from an experimental data and the instrument function. Eliminating an effect of the instrument function from an experimental image is equivalent to eliminating an effect of an objective lens from an experimental image, and thus corresponds to a Cs-correction in STEM by means of image processing software. Among various techniques proposed for deconvolution Maximum Entropy Method (MEM) and Richardson-Lucy Algorithm (RLA) are most popular. For STEM-HAADF imaging Pennycook and his coworkers applied a MEM technique developed in astronomy, where an object function is a point like star. They used a Gaussian and Lorentzian for a probe function, and concluded that a shape of the probe is not important [6]. However, our deconvolution procedure for DigitalMicrograph dedicated to STEM-HAADF (DeConvHAADF) [7] does not assume a point like object, and a good estimate of a probe function is essentially important. The MEM and RLA procedures adopted in DeConvHAADF deduce a solution by changing an estimate function iteratively in such a way that a convolution integral between the estimate function and the probe function reproduces the experimental image. Thus, we can estimate an object function with negligible noise, when we stop the iteration at an appro-

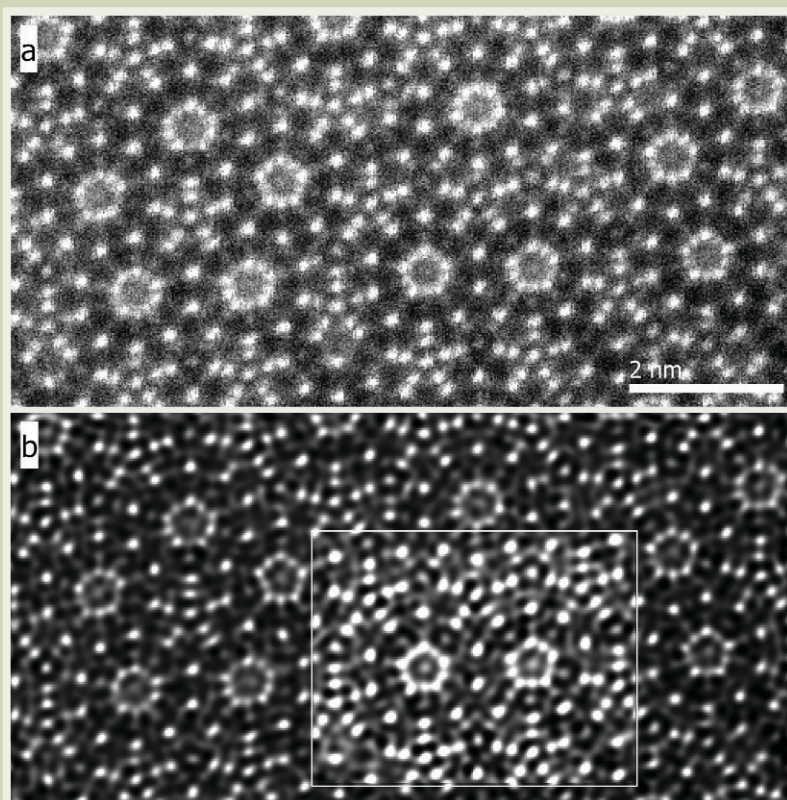


Fig.1 Resolution improvement of STEM-HAADF image using deconvolution.

- (a) STEM-HAADF image of a decagonal quasi-crystal  $\text{Al}_{64}\text{Cu}_{22}\text{Co}_{14}$  taken with JEM-2100F equipped with CEOS Cs-corrector for STEM.
- (b) Result of a MEM deconvolution. Contrast is adjusted in a rectangle box to enhance weak peaks. Probe conditions: Cs=0mm, 24-mrad convergence angle, defocus=0; Gaussian demagnified source with FWHM of 2 pixels; Gaussian focus spread with FWHM of 5 nm.

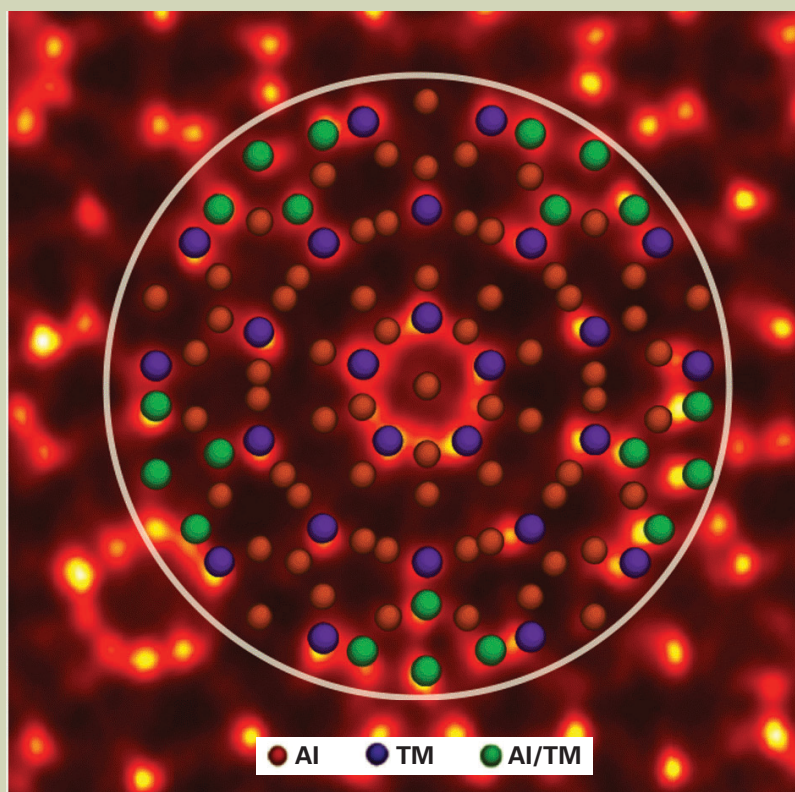


Fig.2 Model structure of decagonal quasi-crystal  $\text{Al}_{64}\text{Cu}_{22}\text{Co}_{14}$ . Cluster model of five-fold symmetry with a diameter of about 2nm. Al represents aluminum, and TM a transition metals, namely Cu or Co. (reproduced from *JEOL News*, Vol.42 (2007) 15 by permission)

prate stage of deconvolution.

Here, we will show an example of deconvolution applied to a STEM-HAADF image of a decagonal quasi-crystal  $\text{Al}_{64}\text{Cu}_{22}\text{Co}_{14}$  (Fig. 1(a)) taken with JEOL JEM-2100F equipped with CEOS Cs-corrector for STEM [8]. If you are interested in details on a sample and its analysis, please consult an original article [9] by the authors who kindly provide this image for our analysis. In the case of Cs-corrected STEM we can extend a convergence angle for probe forming lens, and thus a resultant probe becomes so small that we have to take care of the size of a physical source demagnetized by a condenser system. Moreover, a large convergence angle means a depth of focus becomes small, and thus we have to consider a focus spread due to chromatic aberration. These two points have been ignored for STEM-HAADF imaging with a conventional STEM without a Cs-corrector. We improved recently a probe function of DeConvHAADF to include these two effects.

Figure 1 (b) shows the result of a MEM deconvolution using a probe obtained for Cs = 0 mm at a just focus with 24-mrad convergence angle. The demagnified source size is approximated by a Gaussian with FWHM of 2 pixels, while a focus spread by a Gaussian with FWHM of 5 nm. Contrast is adjusted in a rectangle box to enhance weak peaks. Salt-and-pepper noise in the experimental image is reduced, and blurred contrast becomes sharp. On the other hand some peaks appear at the places where the experimental image does not show clear evidence of their existence. However, we may note that the result of deconvolution including the latter peaks satisfies the experimental image, and seems to correspond to an expected average structure of decagonal quasi-crystal shown in Fig. 2 [9].

## Single Atom Detection by Noise Suppression

Figure 3 (a) shows a STEM-HAADF image of PtRu catalyst particles on carbon support taken with JEM-2100F equipped with CEOS Cs-corrector for STEM [9]. As you can see from this figure aperiodic material such as carbon film gives pixel-wise random noise in a STEM-HAADF image. We have demonstrated that deconvolution is effective to improve resolution of a STEM-HAADF image, namely to correct a spherical aberration of a probe forming lens. It is also effective to reduce the pixel-wise random noise as we will describe in this section. This is because an observed image is given by a convolution integral between an object function and a probe function, and thus each pixel of the observed image should not be absolutely random.

When we continuously observe PtRu catalyst particles, a bright spot occasionally migrates from a border of a PtRu particle. The bright spot is believed to be a single atom of Pt or Ru. Figure 4 (a) is an intensity profile along the line connecting two bright spots indicated by red arrowheads in Fig. 3 (a). We can recognize the presence of these bright spots from a STEM image, when weak intensity is enhanced as in Fig. 3 (a). However, it is difficult to determine a strength and size of the



bright spot from the line profile, since a random noise is so severe. Figure 4 (b) corresponds to a line profile of the image, where the random noise is reduced by  $3 \times 3$  local average. Here, the existences of the particles become clear, but a reduction of peak height and an increase of peak width (FWHM = 0.125 nm) are unavoidable. Figure 3 (b) reproduces a result of deconvolution of the image, where a raw image is pre-smoothed by convolution with a Gaussian of 3-pixel FWHM in order to reduce a random noise, and then the result was deconvoluted with both the probe function used for a quasi-crystal above and the Gaussian used for pre-smoothing simultaneously. Figure 4 (c) is a corresponding line profile obtained from Fig. 3 (b). Here, the random noise in the original image turns into a smoothly varying background, while the peak

heights become higher than those in the original image. An increase of the peak height is a consequence of peak sharpening (FWHM = 0.11 nm) due to deconvolution. Peak heights of these two peaks are close to each other, and also close to a peak height of a bright spot (indicated by a red arrowhead) at the border of a PtRu particle, which is probably a single atom. Therefore, these two spots seem to correspond to a single Pt atom.

If we assume a contrast ratio of Pt and Ru atom is proportional to a square of atomic number ratio (44/78), the contrast ratio of Pt and Ru becomes 0.32. Thus a peak height of Ru atom will be about two-times of a background variation of Fig. 4 (c). Then, a spot whose peak height is significantly higher than the background fluctuation, and also lower than Pt peaks, may correspond to a single Ru

atom as indicated by a yellow arrowhead.

## Measurement of Lattice Distortion and Column Intensity

Occasionally, we want to quantitatively measure intensity of each column of a lattice image for such a case to identify constituent atoms of the columns. However, measuring intensities at many column positions manually to get a statistical estimation is a laborious work. On the other hand a number of techniques to measure lattice distortion from a single lattice image with accuracy of an order of 1% (absolute distortion of an order of pm) were proposed, and some of them were made available commercially. GPA (Geometrical Phase Analysis) [10] is one of such plug-in,

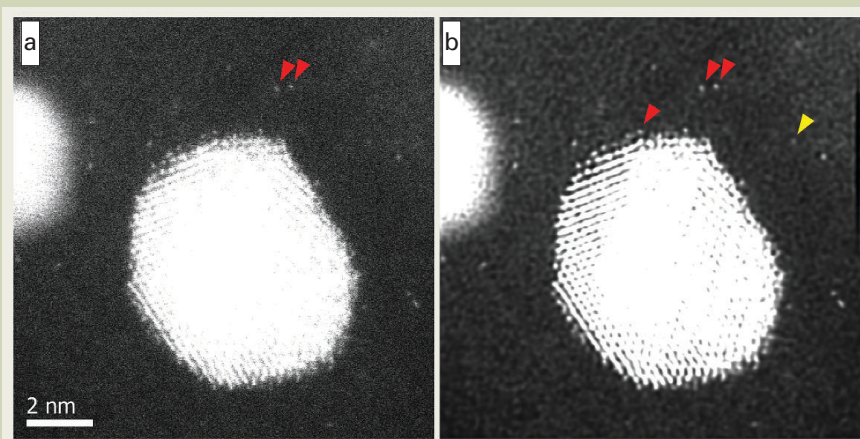


Fig.3 Noise reduction of STEM-HAADF image using deconvolution.

- (a) STEM-HAADF image of PtRu catalyst particles on a carbon support taken with JEM-2100F equipped with CEOS Cs-corrector for STEM. The presence of the bright spots can be recognized from a STEM image, when weak intensity is enhanced. However, it is difficult to determine a strength and size of the bright spot, since a random noise is so severe.
- (b) Result of a MEM deconvolution. A raw image was smoothed by convolution with a Gaussian of 3-pixel FWHM in order to reduce a random noise, then the result was deconvoluted with both the same probe function used for a quasi-crystal and the Gaussian used for pre-smoothing. Random noise is reduced, and the bright spots become clear. Red arrow head may represent a single Pt atom, while yellow arrow head a single Ru atom.

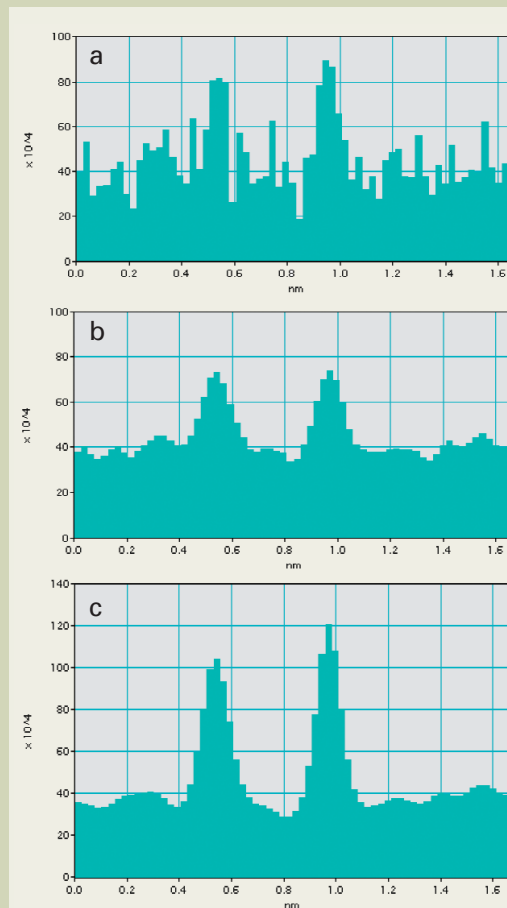


Fig.4 Intensity profiles over bright spots in STEM-HAADF image.

- (a) Intensity profile along the line connecting two bright spots indicated by red arrowheads in Fig. 3 (a). It is difficult to determine a strength and size of the bright spot from the line profile, since a random noise is so severe.
- (b) Line profile of the image where the random noise is reduced by local average. Here, the existences of the particles become clear, but a reduction of peak height and an increase of peak width are unavoidable.
- (c) Line profile of the image where the random noise is reduced with MEM deconvolution. Here, the random noise turns into a smoothly varying background, while a peak height becomes higher than that in the original image. The peak heights of two peaks are close to each other, and these peaks probably correspond to single Pt atoms.

which will be briefly introduced in Other Plug-ins section. In this section we will introduce another strain measurement plug-in called PPA (Peak Pair Analysis) [11] in reference to a STEM-HAADF image of GaAs. PPA estimates lattice strain from a change of distance between column pairs after automatically determining column positions. Since PPA determines column positions, it is easy to get intensity statistics of different columns by automatically measuring intensity at each column position.

**Figure 5** (a) shows a STEM-HAADF image of GaAs [100] taken with JEM-2100F equipped with CEOS Cs-corrector for STEM. If we look carefully the image with a help of red reference lines, we can detect slowly varying image distortion. A STEM-HAADF image often shows this kind of distortion owing to

such as specimen charge-up from electron irradiation and so on, even when probe scanning is stable. This kind of image distortion can be measured as a lattice deformation. Then, we can rectify image distortion using information on lattice deformation, when actual specimen deformation is negligible. Figure 5 (b) shows pseudo-color variations of x- and y-components of lattice vectors in two directions as a function of image position. Using this information we can rectify a deconvoluted image as shown in Fig. 5 (c). In this image all columns align along straight lines, and it is clear that slowly varying image distortion is corrected.

Since relative relations of all column positions are known, intensity of each column position within a specified region will be automatically measured, when we specify only one

column position for Ga and As. **Figure 6** (a) to (c) show histograms of peak intensities at Ga, As and both column positions, respectively. Average intensity at Ga is  $3.42 \times 10^6$  ( $\sigma = 1.9 \times 10^5$ ), while at As is  $3.84 \times 10^6$  ( $\sigma = 2.0 \times 10^5$ ). Thus, we can significantly discriminate intensities at Ga and As, and determine a polarity of GaAs from a STEM-HAADF image. Although we have to examine a size of background of this image, which is a recent hot topic of STEM-HAADF imaging [12], the relative intensity between Ga and As is 1.12, which is close to a square of atomic number ratio (33/31).

## Verification of Cs-correction Using Software

If spherical aberration is present, electrons

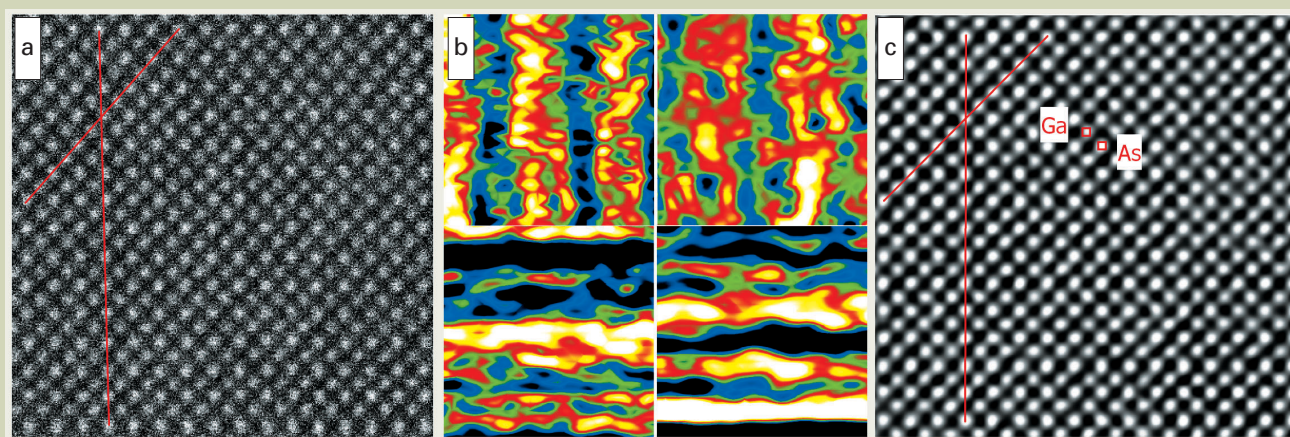


Fig.5 Measurement of lattice distortion and column intensity.

- (a) STEM-HAADF image of GaAs [100] taken with JEM-2100F equipped with CEOS Cs-corrector for STEM. If we look carefully the image with a help of red reference lines, we can notice slowly varying image distortion.
- (b) Pseudo-color display of variations of x- and y-components (left and right columns) of two lattice vectors close to horizontal and vertical directions (upper and lower rows) as a function of image position. FWHM's of these variations are about 2 pixels for lattice vectors of about 25 pixels. A variation of y-component of vertical lattice vector (lower right) is most significant, which corresponds to a change of a scan line distance.
- (c) Deconvoluted image corrected for distortion using information on positional variation of lattice vectors as shown in (b). Atomic columns align on straight lines, and slowly varying image distortion is rectified. Here, intensity difference between Ga and As becomes more apparent than that in the original image.

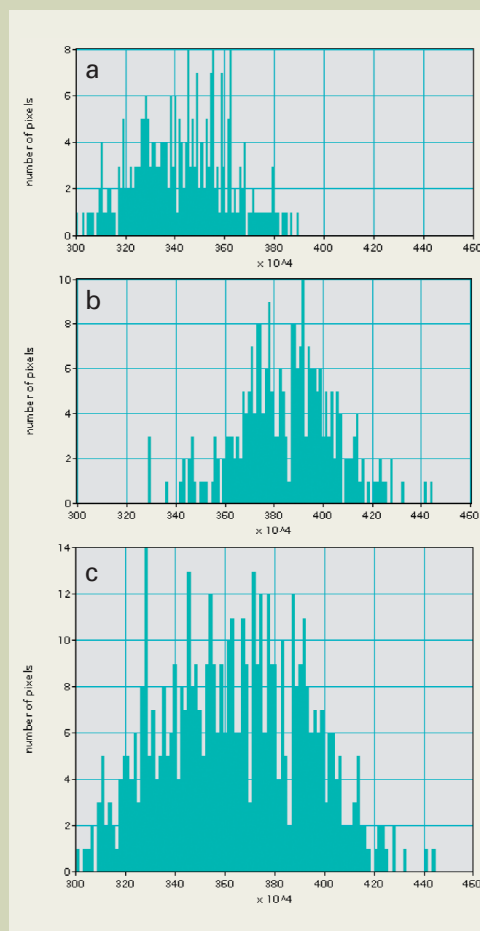


Fig.6 Intensity distributions of atomic columns of Ga and As.

Intensity of each column of Ga and As is automatically measured using information on relative lattice positions. (a), (b) and (c) show intensity histograms of Ga, As and both columns, respectively. Ga intensity is  $3.42 \times 10^6$  ( $\sigma = 1.9 \times 10^5$ ), while As  $3.84 \times 10^6$  ( $\sigma = 2.0 \times 10^5$ ).



scattered into high angle appear on the image plane displaced from an image corresponding to a transmitted wave. This is the reason why sets of lattice fringes appear outside of a particle, when we take an image of small particles. Likewise, lattice fringes extend into vacuum beyond a surface, or into other domain across an interface. One of the advantages of a Cs-corrected CTEM is such that this kind of image delocalization disappears, and a structure at a surface/interface becomes clear. Another advantage is such that a phase contrast from a specimen support, like a carbon film, which is a phase object, is suppressed, and observation of fine particles becomes easier. These advantages can be derived from correcting spherical aberration with software using a series of CTEM images. Moreover, software Cs-correction has further benefits over hardware Cs-correction as shown below.

Here, we will demonstrate that delocalization of lattice fringes on a CTEM image of Au particles disappear, and thus verify that software Cs-correction is in fact possible. We reconstruct here a wave front using FSR (Focal Series Reconstruction) function of FTSR (Focal and Tilt Series Reconstruction) plug-in. FTSR uses a specially designed Wiener filter[2] to estimate a wave front assuming the linear imaging that is valid when a transmitted wave is stronger than diffracted waves. Since the Wiener filter takes into account wave aberration, we can get a Cs-corrected wave front at a specimen exit surface.

**Figure 7** (a) reproduces a CTEM image of nano-meter scale Au particles on carbon support taken with JEM-2100F ( $C_s = 0.5$  mm). This image is selected from a through-focus series of 20 images (a defocus step is about 9 nm) to be used for Cs-correction, and a defocus value is about -46 nm (under focus). An

enlarged image (Fig. 7 (b)) of one spherical particle (about 6.5 nm) located at the center right clearly demonstrates sets of lattice fringes that appear outside of the particle. An expected displacement of a diffracted image for (311) reflection is 3.3 nm at this defocus. Figure 7 (c) and (d) are respectively an amplitude and phase distributions of the wave function at the specimen exit surface obtained from the through-focus series of 20 images. Spherical aberration was corrected assuming  $C_s = 0.5$  mm. In addition, an estimated two-fold astigmatism of 5.9 nm was also corrected. Displaced lattice fringes observed in original images disappeared, and thus we can conclude that spherical aberration has been corrected successfully. The amplitude image corresponds to a just-focus image taken with a Cs-corrected CTEM. Here, phase contrast from carbon support is suppressed and thus observation of fine particles becomes as easy as a hardware Cs-corrected image.

The phase image shown in Fig. 7 (d) seems to be polluted when compared with the amplitude image. However, this is because carbon support film that is a phase object is faithfully observed here. The phase distribution of the wave function at the specimen exit surface obtained by using software is an aberration free image up to an information limit (diffraction limit), even though very low frequencies cannot be recovered. FTSR includes TSR (Tilt Series Reconstruction) function that uses the images obtained by tilting the beam at six directions. It is possible using TSR to reconstruct a wave front with a super resolution, which exceeds the information limit of an axial illumination.

When observing a phase object using a Cs-corrected CTEM the spherical aberration is not completely corrected, but adjusted from a few

microns to tens of microns, and then a defocus is tuned to a Scherzer focus corresponding to the adjusted  $C_s$ . This imaging condition in principle corresponds to a regular imaging condition proposed by Scherzer [13], although a spherical aberration is far smaller than that of a regular microscope. This means that an image taken at the Scherzer focus using a Cs-corrected CTEM is not an aberration free image. In order to observe a phase object using a Cs-corrected CTEM under an aberration free condition, wave front reconstruction using a series of through-focus images may be performed in the same way as applied to a regular CTEM. Here, attenuation of a phase contrast transfer function is also recovered at all frequencies except very low scattering angles, and thus an image with higher contrast than an unprocessed image will be obtained.

## Observation of Oxygen with Software Cs-correction

It is widely accepted that a STEM-HAADF image can be interpreted easier than a CTEM image, since the contrast of a STEM-HAADF image does not reverse with a sample thickness nor defocus change, while a CTEM image does. Moreover discrimination of element is easy using a STEM-HAADF image, since a contrast is proportional to a square of atomic number. However, STEM-HAADF is not suitable to detect a light atom. It may be noted that if we correct aberration using software and estimate wave function at the specimen exit surface, the wave function does not depend on a defocus as a CTEM image. Moreover, if a specimen is thin enough, a phase distribution approximately reflects a projected potential of a specimen, and thus it becomes possible to detect a light atom and a

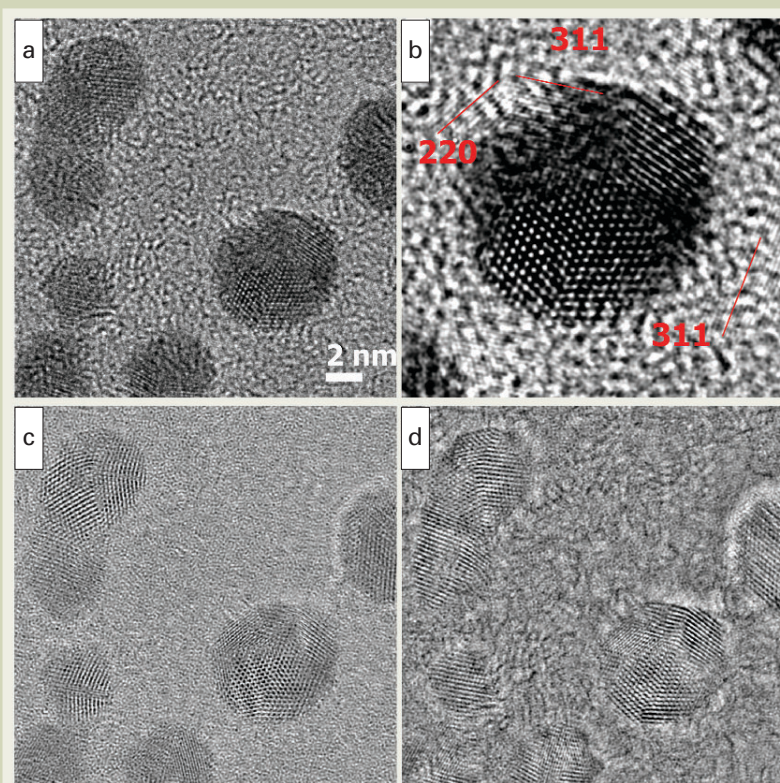


Fig.7 Verification of Cs-correction with software.

- (a) CTEM image of nano-meter scale Au particles on carbon support taken with JEM-2100F ( $C_s=0.5$ mm). Defocus value of this image is about -46 nm, and sets of lattice fringes appear outside of particles.
- (b) Magnification of a spherical particle (about 6.5 nm) at the center right of (a), where (311) and (220) lattice fringes that appear outside of the particle are evident. A plug-in, HREM-Filters Pro, is used to clarify the lattice fringes by suppressing aperiodic noise.
- (c) and (d) Amplitude and phase distributions at the specimen exit surface obtained from the through-focus series of 20 images. Spherical aberration (0.5 mm) and estimated astigmatism (5.9 nm) are corrected here. Delocalized lattice fringes observed in the original images are vanished, which is a verification of spherical aberration correction. Amplitude image in (c) suppresses phase contrast from carbon support, and thus observation of fine particles becomes as easy as a hardware Cs-corrected image. On the other hand the phase image in (d) faithfully shows carbon support under the aberration-free condition.



specimen structure can be estimated more easily.

In this section we will try to detect oxygen in  $\text{SrTiO}_3$ . Figure 7 (a) shows an image of  $\text{SrTiO}_3$  [001] taken with JEM-2100F ( $C_s = 0.5$  mm) at around the Scherzer focus. A through-focus series of 20 images (a defocus step is about 9 nm) is acquired from this sample. Figure 7 (b) and (c) are respectively an amplitude and phase distributions of the wave function at the specimen exit surface obtained from the 20 through-focus images. They correspond to an area in the box indicated in Fig. 7 (a) close to the specimen edge. A spherical aberration of 0.5 mm is corrected in the same way as applied to the case of Au particles before. In addition, an estimated two-fold astigmatism of 4.9 nm was also corrected. The phase image close to the specimen edge shows a pattern corresponding to a structure model shown in the figure. Here, Sr and Ti-O columns show almost the same contrast. A weak contrast (red circle) at the center of a square made of Sr and Ti-O corresponds to oxygen. A dark contrast just inside of the sample along the sample edge is an equal thickness fringe. Since the first equal thickness fringe of this sample appears at a thickness of about 5 nm, a sample thickness should be less than 5 nm to obtain a phase image that simply reflects the model structure.

## Brief Introduction of Other Plug-ins

Here, we will briefly introduce other plug-ins for quantitative electron microscopy developed at HREM Research for DigitalMicrograph.

- ◆ *DeConvEELS* improves an energy resolution of an EELS spectrum using the same principles used in DeConvHAADF [7, 14]
- ◆ *IWFR* (Iterative Wave Function Reconstruction) corrects spherical aberration for CTEM using a set of images. Contrary to FTSR this plug-in estimates a wave function at a specimen exit surface using an iterative algorithm. Normally, IWFR requires a fewer number of images to estimate the wave function than FTSR [3].

◆ *GPA* (Geometrical Phase Analysis) estimates lattice distortion from a single lattice image. Contrary to PPA this plug-in determines lattice distortion from phase distributions of the images separately calculated by inverse Fourier transform of different diffraction spots in a Fourier transform of the lattice image [10].

◆ *QPt* (Quantitative Phase Technology) estimates a phase distribution from two or three images based on the so-called transport intensity equation [15]. An electromagnetic field over a large area can be measured without an electron bi-prism and a vacuum reference area required by electron holography. On the other hand a spherical aberration can be corrected using phase information estimated from high-resolution images. Application of this technique to phase contrast microscopy of biological materials is anticipated in future [16, 17].

◆ *HREM-Filters* enhances periodic structure by reducing a contribution of aperiodic structure from the image (specimen support, quantum noise, etc). This plug-in is especially useful for the image of non-ideal periodic structure, where there are crystals with different orientations, a periodicity changes in direction, an image has distortion, and so on.). The periodicity is effectively enhanced by applying a Fourier filter, such as a Wiener filter, to each small area where a periodicity is uniform [18].

## Conclusions

Quantitative electron microscopy using plug-ins developed for DigitalMicrograph (Gatan) has been demonstrated by making use of the data taken with JEM-2100F. By analyzing the data quantitatively we can deduce information from an observed data, which is hard to be detected by human eyes. Thus, we can add a new value to the observed data. We would like to encourage all the readers who have DigitalMicrograph on their microscope, to dig out useful information by quantitative electron microscopy from the data at hand.

The authors would like to thank to Prof. E. Abe, The University of Tokyo for giving us a

permission to use a quasi-crystal data.

## References

- [1] W. Coene A. Thust, M. Op de Beeck, and D. van Dyck, *Ultramicroscopy* **64** (1996) 109.
- [2] R. Meyer, A. Kirkland and W. Saxton, *Ultramicroscopy* **92** (2002) 89.; R. Meyer, A. Kirkland and W. Saxton, *Ultramicroscopy* **99** (2004) 115.
- [3] L.J. Allen, W. McBride, N.L. O'Leary and M.P. Oxley, *Ultramicroscopy* **100** (2004) 91.
- [4] Gatan, Inc. [www.gatan.inc](http://www.gatan.inc)
- [5] S.J. Pennycook and D.E. Jesson, *Ultramicroscopy* **37** (1991) 14.
- [6] A.J. McGibbon, S.J. Pennycook and D.E. Jesson, *J. of Microscopy* **195** (1999) 44.
- [7] K. Ishizuka, *Microsc Microanal* **11** (2005) 1430.
- [8] M. Haider, H. Rose, S. Uhlemann, E. Schwan, B. Kabius and K. Urban, *Ultramicroscopy* **75** (1998) 53.
- [9] S. Taniguchi and E. Abe, *Phil. Mag.* (2008) in press.
- [10] M.J. Hytch, E. Snoeck and R. Kilaas, *Ultramicroscopy* **74** (1998) 131.
- [11] P.L. Galindo, S. Kret, A.M. Sanchez, J.-Y. Laval, A. Yanez, J. Pizarro, E. Guerrero, T. Ben, S. Molina, *Ultramicroscopy* **107** (2007) 1186.
- [12] D.O. Klenov and S. Stemmer, *Ultramicroscopy* **106** (2006) 889.
- [13] O. Scherzer, *J. Appl. Phys.* **20** (1949) 20.
- [14] K. Ishizuka, K. Kimoto and Y. Bando, *Microsc Microanal* **9** (2003) 832; K. Ishizuka, *Kenbikyoku* **39** (2004) 204 (in Japanese).
- [15] M.R. Teague, *J. Opt. Soc. Am.* **73** (1983) 1434.
- [16] K. Ishizuka and B. Allman, *J. Electron Microsc.* **54** (2005) 191.
- [17] K. Ishizuka, *Microsc Microanal* **11** (2005) 2160; K. Ishizuka, *Kenbikyoku* **40** (2005) 188 (in Japanese).
- [18] K. Ishizuka, P.H. C. Eilers, T. Kogure, *Microscopy Today* 2007, 16.

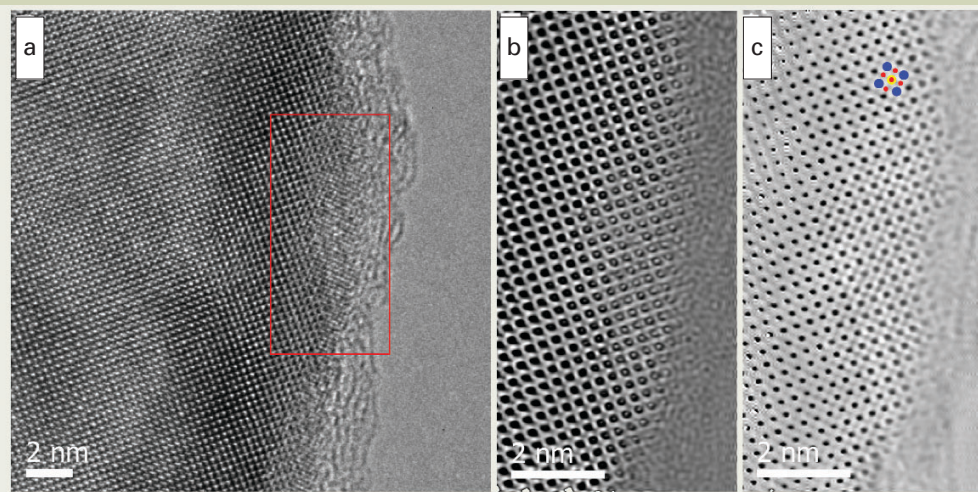


Fig.8 Observation of oxygen with software Cs-correction.

- (a) CTEM image of  $\text{SrTiO}_3$  [001] taken with JEM-2100F ( $C_s = 0.5$  mm) close to the Scherzer focus. An equal thickness fringe is observed just inside of the sample along the sample edge.
- (b) and (c) Amplitude and phase distributions at the specimen exit surface obtained from the through-focus series of 20 images. They correspond to an area inside of the rectangle box shown in (a). Contrast corresponding to the model structure is observed in the phase image close to the specimen edge, whose thickness is less than the one yielding the equal thickness fringe. In the structure model, blue, yellow and red circles represent Sr, Ti and oxygen, respectively. Weak contrast at the center of the square made of Sr and Ti-O corresponds to oxygen.